LIBX-A401: A Novel Selective Inhibitor of Acyl-CoA Synthetase Long Chain Family Member 4 (ACSL4) and Its Binding Mode

Darius Mazhari Dorooee,[1] Séverine Ravez,[2] Didier Vertommen,[3] Nicolas Renault,[4] Nicolas Papadopoulos,[5,6,7] Romain Marteau,[1] Emeline Charnelle,[2] Karine Porte,[1] Alexandre Gobert,[2] Nathalie Hennuyer,[8] Gaetan Herinckx,[3] Bart Staels,[8] Patricia Melnyk,[2] Stefan N Constantinescu,[5,6,7,9] Raphaël Frédérick,[1*] Jamal El Bakali[2*]

[1] Medicinal Chemistry Research Group (CMFA), Louvain Drug Research Institute (LDRI), Université Catholique de Louvain, 73 Avenue Mounier, B1.73.10, 1200, Brussels, Belgium.

[2] Univ. Lille, Inserm, CHU Lille, UMR-S-U1172 - LilNCog - Lille Neuroscience & Cognition, F-59000 Lille, France.

[3] MASSPROT Platform, de Duve Institute, Université Catholique de Louvain, Brussels, Belgium.

[4] INSERM, CHU Lille, U-1286 - INFINITE - Institute for Translational Research in Inflammation, Université de Lille, F-59000 Lille, France.

[5] Ludwig Institute for Cancer Research, Brussels, Belgium.

[6] de Duve Institute, Université catholique de Louvain, Brussels, Belgium.

[7] WEL Research Institute, WELBIO Department, Wavre, Belgium.

[8] Univ. Lille, Inserm, CHU Lille, Institut Pasteur de Lille, U-1011-EGID, F-59000, Lille, France.

[9] Ludwig Institute for Cancer Research, Nuffield Department of Medicine, Oxford University, Oxford, United Kingdom.

*Corresponding authors. Jamal El Bakali, e-mail: jamal.el-bakali@univ-lille.fr, Raphaël Frédérick, e-mail: raphael.frederick@uclouvain.be

KEYWORDS: Acyl-coenzyme A synthetase long-chain family member 4 (ACSL4), Cancer, Chemical biology, Ferroptosis, Hydrogen Deuterium Exchange (HDx) mass spectrometry, Lipids, Medicinal chemistry, Photoaffinity labeling, Rosiglitazone.

ABSTRACT

Lipid metabolism affects many cellular processes essential for homeostasis, and its disruption is linked to various diseases. A key enzyme in these processes, acyl-coenzyme A synthetase long-chain family member 4 (ACSL4), is a promising target for treating conditions involving ferroptosis and certain cancers. Rosiglitazone (ROSI) is a known ACSL4 inhibitor but its potent activity on peroxisome proliferator-activated receptor gamma (PPARγ), a nuclear receptor strongly involved in lipid metabolism constitutes an important limitation. This study focuses on developing novel ACSL4 inhibitors derived from ROSI, which lack PPARγ activity. Binding of the most potent compound of this series (**9**) relies on the prior binding of ATP. Hydrogen-Deuterium Exchange Mass Spectrometry (HDx-MS) demonstrated that ATP binding stabilizes the ACSL4 *C*-terminus, an effect enhanced by compound **9**, which also alters important peptide sequences, including the fatty acid gate-domain. Photoaffinity Labeling (PAL) with a diazirine-based probe identified residue A329 in the fatty acid pocket. Molecular dynamics simulations and site-directed mutagenesis highlighted Q302 as critical for compound **9** binding. Thus, compound **9** (**LIBX-A401**) is a promising tool for studying ACSL4 in ferroptosis-related diseases and cancer, and the elucidation of its binding mode paves the way to the rational design of optimized inhibitors.

GRAPHICAL ABSTRACT

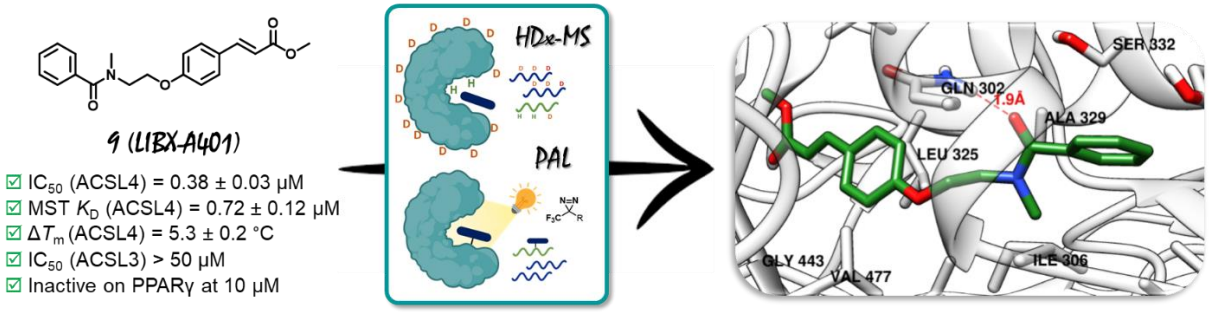

INTRODUCTION

Lipid metabolism encompasses a series of dynamic and interdependent processes that regulate the synthesis, storage, and use of lipids in living organisms. Within this complex set of biochemical processes, the acyl-coenzyme A (Acyl-CoA) synthetase long-chain family of enzymes (ACSLs) plays a pivotal role in the activation of long-chain fatty acids into corresponding fatty acyl-CoA esters. Once activated, fatty acids (FAs) participate in various cellular pathways including the synthesis of phospholipids, triacylglycerol and cholesterol esters, β-oxidation and protein acylation.[1] In mammals, the ACSL family comprises five members, ACSL1 and ACSL3-6, which have different tissue and subcellular distributions, and substrate preferences.[2] They have all been identified as potential therapeutic targets in various diseases.[3] More specifically, ACSL4 recently emerged as an attractive target in some cancers including hepatocellular carcinoma,[4] estrogen receptor-negative breast cancer,[5] and prostate cancer.[6] In addition, because of its marked preference for polyunsaturated fatty acids (PUFAs) activation, ACSL4 has been identified as a pivotal contributor to ferroptosis,[7] an iron-dependent regulated cell death marked by extensive membrane lipid peroxidation.[8] Notably, ACSL4 plays a key role in enriching membrane phospholipids (PLs) with PUFAs, which are highly prone to peroxidation.[7c],[9] Moreover, its phosphorylation by Protein Kinase C βII (at T328) was shown to promote its dimerization leading to the amplification of lipid peroxidation and subsequent ferroptosis.[10] Interestingly, genetic depletion or pharmacological inhibition of ACSL4 confers a strong protection against ferroptosis.[7c] Therefore inhibiting ACSL4 may have a positive impact on diseases or conditions in which ferroptosis is involved as well as in certain cancers. So far, no potent, selective and well-validated ACSL4 inhibitor has been described. The most widely used ACSL4 inhibitor is rosiglitazone (ROSI) which selectively inhibits ACSL4 (over other ACSLs) in the micromolar range.[11] However, its potent activity on peroxisome proliferator-activated receptor gamma (PPARγ), a nuclear receptor strongly involved in lipid metabolism constitutes an important limitation.

Although mammalian ACSLs have been thoroughly biochemically characterized, structural information is missing with the only known structure of ACSL being the one of *Thermus thermophilus tt*LC-FACS.[12] Despite sharing only about 20% sequence identity (37% sequence similarity) with human ACSL4, this structure provides the first

glimpse into the ACSL architecture and mechanism of catalysis. Indeed, this bacterial ACSL acts as a dimeric complex of two identical subunits displaying a large *N*-terminal domain linked via a six amino acid linker to a relatively short flexible *C*-terminal domain with the active site located at the domain interface. An important feature in the structure of ACSL is the presence of a FA gate-domain, whose sequence (D-x4-Y/W-LPLAH-x2-E) is highly conserved in mammals.[13] Interestingly, *tt*LC-FACS was shown to function through a Bi Uni Uni Bi ping-pong mechanism, where ATP binds first inducing the opening of the FA tunnel allowing FA binding and subsequent acyl-AMP formation and PPi release.[12] In the second step, CoA reacts with acyl-AMP to generate acyl-CoA and AMP as products. These mechanistic and structural data are crucial for understanding the functioning of human ACSLs. However, the specific intricacies of ACSL's architecture and their ligand-binding sites remain largely unknown.

Hydrogen-Deuterium Exchange Mass Spectrometry (HDx-MS) and photoaffinity labeling (PAL) are powerful techniques contributing to the elucidation of structural basis of important proteins. HDx-MS provides a dynamic view of the conformational changes in proteins upon inhibitor binding and could help identify potential binding regions.[14] On the other hand, PAL enables the covalent attachment of a probe to the protein target, allowing for precise mapping of the ligand-binding site.[15]

Here, we report (*i*) the medicinal chemistry approach around ROSI leading to sub-micromolar range inhibitors of human ACSL4 devoid of PPARγ activity and (*ii*) the chemical biology approach, combining HDx-MS and PAL to gain structural insights into the binding mode of these inhibitors.

RESULT AND DISCUSSION

In order to draw early structure-activity relationship (SAR), ROSI analogues were purchased or readily synthesized as described in Scheme S1. Inhibitory activity was evaluated on the human recombinant ACSL4 using the Enzchek® pyrophosphate assay as previously described.[16] Thus, we started our SAR study by evaluating commercial thiazolidinedione analogues and by modulating the western side chain of rosiglitazone (Table S1). Building upon these initial modulations, we selected ROSI (Compound **1**, IC_{50} = 1.1 µM) and its phenyl analogue (Compound **2**, IC_{50} = 0.4 µM)

as the starting points for further SAR investigations (Table 1, Schemes S2 and S3). Our goal was to enhance the inhibitory activity against ACSL4 while minimizing the effect on PPARγ. Our initial step involved removing the thiazolidinedione ring, a key moiety responsible for the PPARγ activity of ROSI. However, this modification resulted in a complete loss of inhibitory activity against ACSL4 (**3**, IC_{50} > 50 µM). Next, *N*-methylation of thiazolidinedione to remove the acidic proton essential for PPARγ activity was performed. Encouragingly, the *N*-methyl analogue (**4**) known to be inactive against PPARγ,[17] retained micromolar-range activity against ACSL4 (IC_{50} = 4.5 µM), hence demonstrating the possibility to abolish PPARγ activity while maintaining the ACSL4 inhibitory potency.

Table 1. SAR investigation around the thiazolidinedione moiety of ROSI. IC_{50} values (± SEM) were determined by three independent experiments performed in duplicate for each compound concentration.

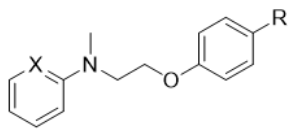

Entry	X	R	ACSL4 IC_{50}, µM
1 (ROSI)	N	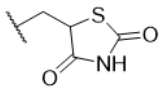	1.1 ± 0.1
2	CH		0.4 ± 0.1
3	N	H	> 50
4	N	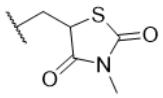	4.5 ± 0.7
5	CH	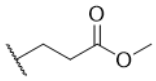	8.5 ± 2.4
6	CH	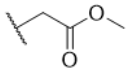	24.1 ± 0.6
7	CH	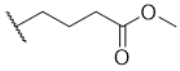	> 50
8	CH	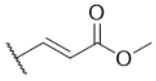	1.5 ± 0.4

Notably, rigidifying the ethylene linker of compound **5** leading to cinnamic derivative **8** restored a potency comparable to rosiglitazone (IC_{50} = 1.5 µM) with high selectivity over ACSL3 (IC_{50} > 50 µM), which shares 63% sequence identity with ACSL4. Remarkably, compound **8** was inactive on PPARγ at 10 µM, in contrast to rosiglitazone, which displays an EC_{50} of 36 nM. Finally, replacing the amine in the linker connecting the two phenyl groups with an amide, resulting in compound **9**, allowed for a further improvement of ACSL4 inhibitory activity (IC_{50} = 0.38 µM, Figure 1), while keeping the same selectivity profile as compound **8**. Compound **9** features a Michael acceptor that may potentially engage in an irreversible mechanism. However, the reversibility of the inhibition was demonstrated using a jump dilution assay.

The binding of compound **9** to ACSL4 was further confirmed using two biophysical techniques, namely nano Differential Scanning Fluorimetry (nDSF) and MicroScale Thermophoresis (MST). As illustrated in Figure 1, no binding event was detected when **9** was tested in the absence of ATP against ACSL4 using these two techniques (Figures 1B and 1C). However, in the presence of a saturating concentration of ATP, a ΔT_m value of 5.3 °C was obtained by nDSF (at 5 µM of cpd **9**) and a K_D value of 0.72 µM was determined by MST. These data indicate that binding of **9** is ATP-dependent, consistent with observations from *tt*LC-FACS, where ATP binding induces the opening of the fatty acid tunnel, facilitating fatty acid binding. Taken together, these findings suggest a similar binding mode for compound **9**.

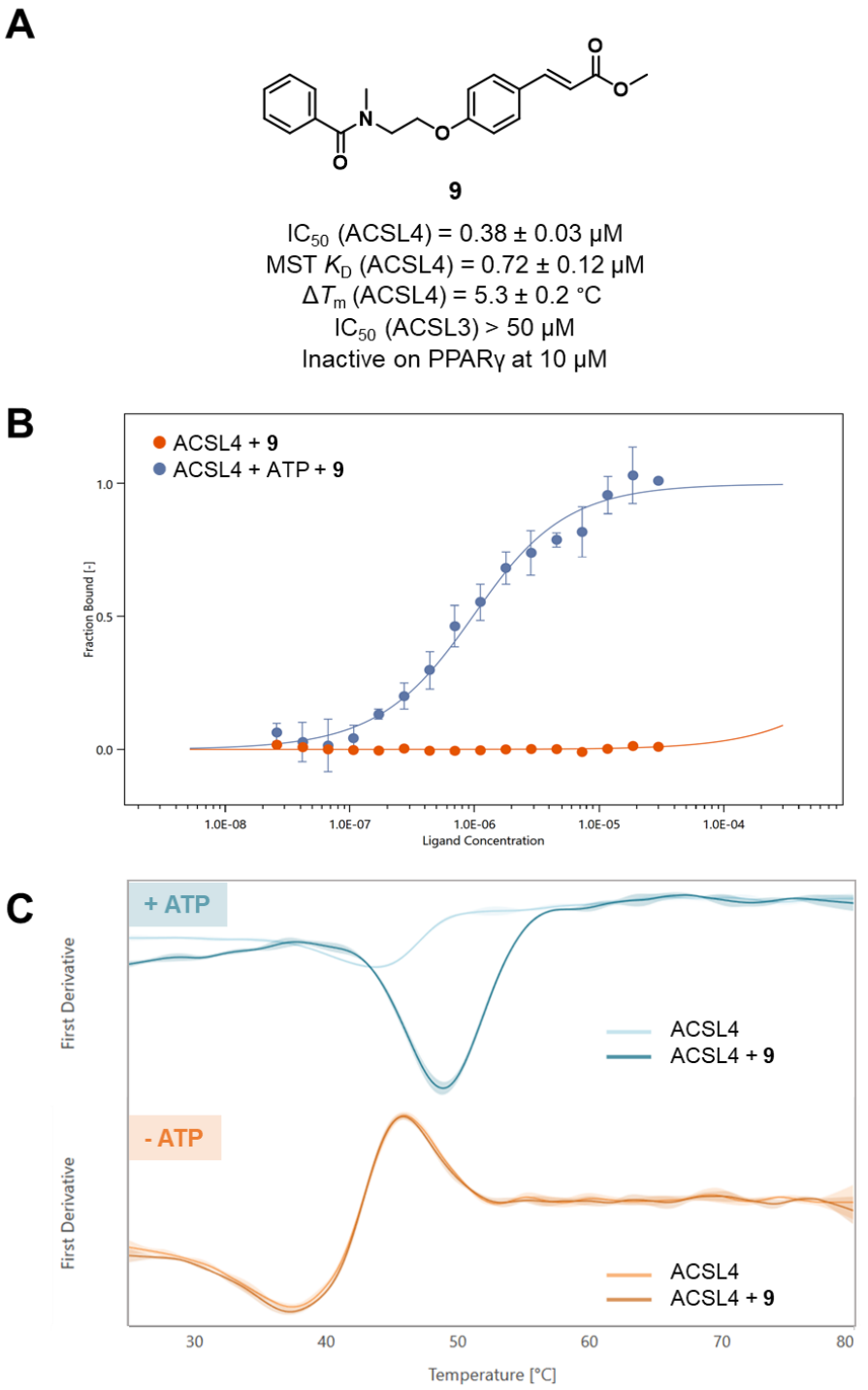

Figure 1. Evaluation of compound **9** against ACSL4. **A**) Structure of **9** and summary of its binding/inhibitory activity profile against ACSL4 as well as its selectivity over ACSL3 and PPARγ. **B**) MST traces, with and without 1 mM ATP (in blue and orange, respectively), showing that the binding of **9** depends on the prior binding of ATP. A K_D value of 720 nM was obtained for **9** in the presence of 1 mM ATP. **C**) nDSF traces with and without 1 mM ATP (in blue and orange, respectively), confirming that ATP is required for the binding of compound **9**. A ΔT_m value of 5.3 °C was obtained for **9** (5 µM) in the presence of 1 mM ATP. K_D and ΔT_m values were determined by three independent experiments for each compound concentration.

In the absence of structural data, we set out to elucidate the binding mode of compound **9**. To this end, two powerful and complementary techniques were used: HDx-MS and PAL. Because of the measurement of deuterium incorporation on the peptide amide backbone by MS, HDx-MS allows for the identification of protein domains that are exposed to solvent and therefore is well suited to unveil protein conformational changes upon ligand binding as well as identifying potential binding sites.[18] The on-column pepsin digestion led to at least 82% of protein coverage with assayed conditions (Figure S1). nDSF confirmed ACSL4 stability at exchange temperature for the longest exchange time (24 h, Figure S2). Because ATP is required for the binding of **9**, we first compared the differences in peptide deuterium intake between ACSL4 with and without a saturating concentration of ATP (400 µM, ACSL4-ATP). The addition of ATP resulted in reduced accessibility of the *C*-terminus domain to deuterium incorporation (Figure S3A), consistent with the literature as ATP binding on *tt*LC-FACS was shown to induce a *C*-terminus domain locking on the *N*-terminus domain.[12] Next, we aimed to investigate the impact of compound **9** binding on the conformation of ACSL4. Consequently, we compared two conditions: one where ACSL4 was incubated with ATP at 400 µM (ACSL4-ATP), and another where ACSL4 was present with both ATP at 400 µM and compound **9** at 25 µM (saturating concentration, ACSL4-ATP-**9**). Figures 2 and S3B indicate that ACSL4-ATP-**9** further reduces the deuterium uptake in the *C*-terminus domain compared to ACSL4-ATP. In addition, the presence of compound **9** resulted in a significant reduction in deuterium uptake on two other sequences: peptide $_{316}$IGYLPLAHVLEL$_{327}$ (peptide A) and peptide $_{371}$MAAVPEIM$_{378}$ (peptide B). Interestingly, peptide A sequence contains the highly conserved FA gate-domain (Figure S4) previously described as important for substrate specificity.[2] The optimized model of ACSL4 presented in Figure 2 shows that the two identified peptides are positioned close to each other and near the *C*-terminus domain, suggesting the possibility of a potential binding site for molecule **9** within this region.

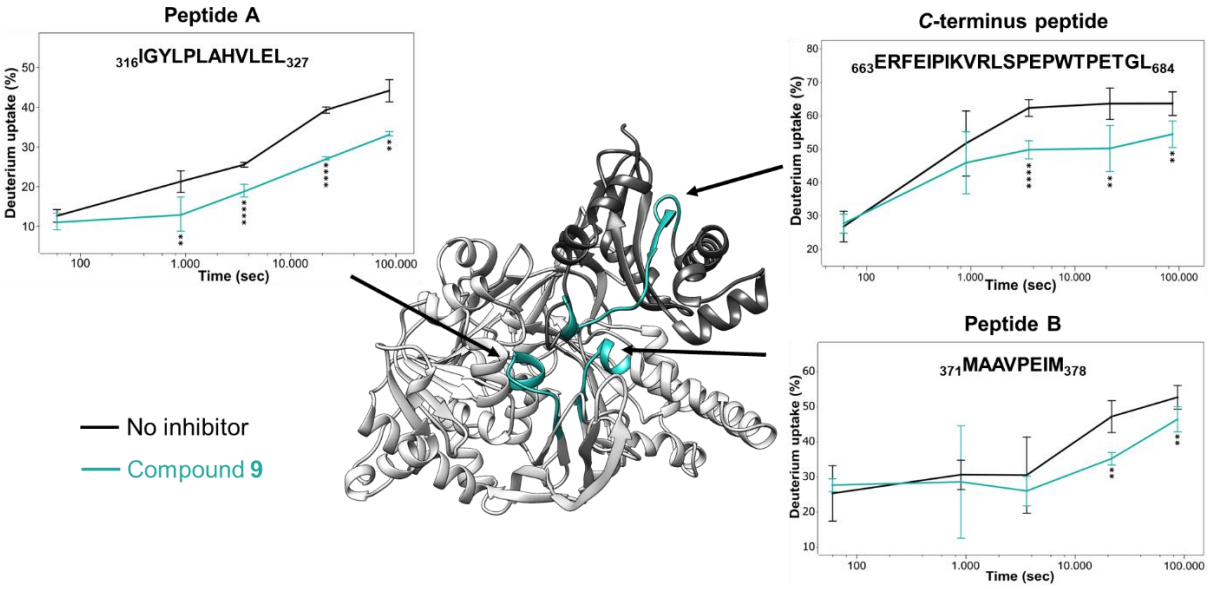

Figure 2. HDx-MS results with compound **9** in the presence of ATP. Changes in deuterium uptake at different exchange times are shown for the identified peptides, themselves illustrated on the ACSL4 model. ACSL4 *C*-terminus and *N*-terminus are depicted in dark grey and white, respectively. Peptides A, B and the closest identified peptide of the *C*-terminus are represented in cyan. Uptake plots for each illustrated peptide show the impact of compound **9** on deuterium incorporation. Peptide traces shown represent mean ± SD of three independent experiments. Statistically significant using HDExaminer, ** $p < 0.01$, *** $p < 0.001$, **** $p < 0.0001$.

To further pinpoint the binding site of compound **9**, we conducted PAL experiments. Based on the SAR (data not shown), we designed an original photoactivable probe introducing a trifluoromethyl diazirine group at the *para* position of the benzamide part on **9** to give the probe **10** (Figure 3A). The latter was synthesized from amine **11** following a standard BOP coupling procedure in the presence of the commercial 4-[3-(trifluoromethyl)-3*H*-diazirin-3-yl]benzoic acid (Scheme S4). Although less potent than **9**, probe **10** retained some inhibitory activity against ACSL4 (IC_{50} = 24.4 µM). Next, ACSL4 was incubated with probe **10** at 100 µM for 30 min, and the photoaffinity labeling was then performed by irradiation at 365 nm for 10 min. To determine the crosslinking site, the samples underwent trypsin digestion, and the resulting peptides were analyzed using nanoUPLC-MS/MS (sequence coverage = 73%, Figure S5). Following this experimental setup, five peptides were detected with an increase in peptide mass of 419.13 Da corresponding to the incorporation of the probe (Figure 3A, Table S2). Interestingly, the peptide with the amino acid sequence $_{313}$DTYIGYLPLAHVLELTAEISCFTYGCR$_{339}$ (Peptide C) comprises the sequence of peptide A identified by HDx-MS. Based on these results, we performed targeted

MS/MS analysis in the presence or absence of 100 µM of competing compound **9** to highlight non-specific labeling. The signal of peptide C was significantly decreased by the addition of **9** (Figure 3B) whereas other identified peptides showed either less significant or no significant decreases (Figure S6).

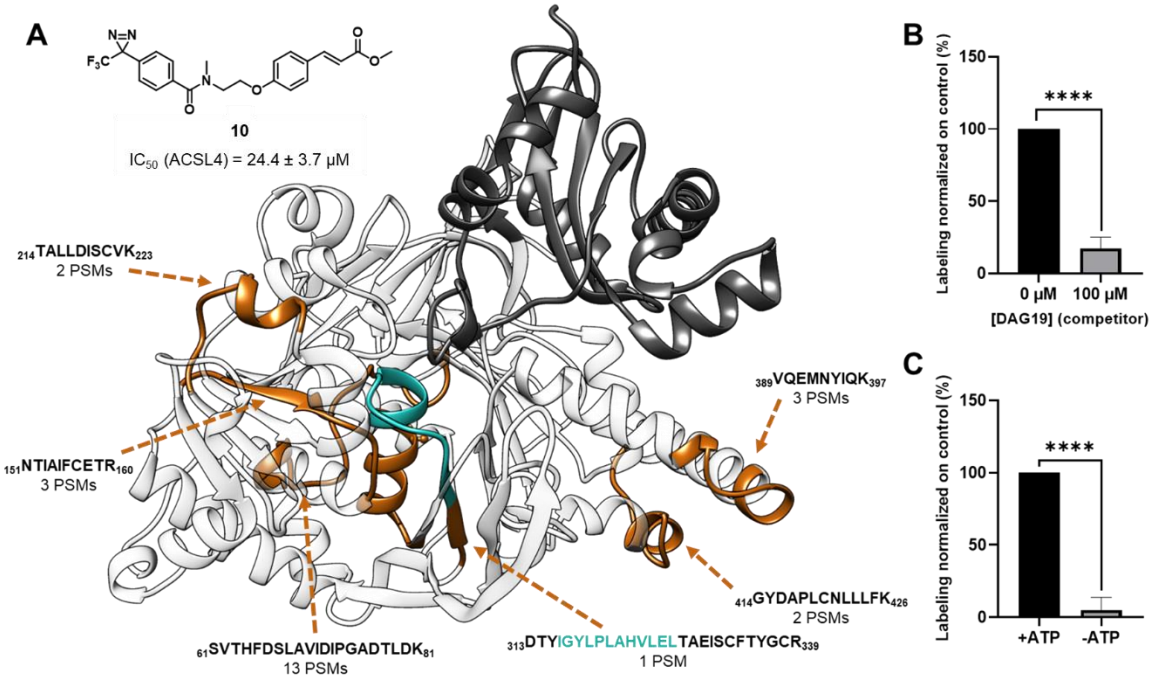

Figure 3. Photoaffinity labeling identification of compound **9** binding site in ACSL4. **A**) Structure of photoaffinity labeling probe **10** and representation of its binding peptides (orange) on ACSL4 model for which the number of peptide-spectrum matches (PSMs) identified are shown. The previously identified peptide A, included in identified peptide C, is represented in cyan. **B**) Results of the competition assay in targeted MS/MS analysis for peptide C with and without compound **9**. **C**) Results of the labeling assay with and without ATP in targeted MS/MS analysis for peptide C. Data shown are representative of three independent experiments. Statistically significant using unpaired t-test, **** $p < 0.0001$.

To validate these results, we measured the labeling of identified peptides with and without ATP as we demonstrated the requirement of ATP for the binding of **9**. The inability to identify peptide C as labeled in the absence of ATP further confirmed the labeling specificity of this peptide (Figures 3C and S6). Finally, analysis of MS/MS fragmentation profile designated A329 as the modified residue of the identified peptide (Figure S7A). It is worth noting that A329 in human ACSL4 aligns with L236 of *tt*LC-FACS (Figure S4) which is located at the distal end of the FA tunnel. Interestingly, mutation of this specific amino acid in the rat ACSL4 to either a glutamate or a glutamine led to a dramatic loss in enzymatic activity.[19]

Building upon these findings, we initiated *in silico* studies to elucidate the binding mode of compound **9**. A BLAST search of PDB templates revealed 16 homologous sequences with at least 50% coverage and 25% sequence identity with human ACSL4. Therefore, we employed AlphaFold 2.0[20] to restrain the extensive set of structural templates to predict the structure of the soluble form of human ACSL4 (42-711). The design of a model for the ACSL4-ligand complex was facilitated by utilizing the unbound state of the AlphaFold model and the conserved ATP position found in homologous PDB structures. Arachidonic acid was selected as the preferential ligand to pinpoint the orthosteric binding pocket through docking and energy refinement, utilizing the arachidonyl-AMP intermediate formed during the enzymatic reaction. Once the arachidonyl-AMP was removed, blind docking experiments were conducted to explore the entire protein. These experiments revealed the best docking pose of **9** within the orthosteric fatty acid binding site, yielding a docking score of -9.76 kcal/mol. Other docking poses were observed (Figure S8) but with docking scores lowered by at least 10%. Interestingly, the best docking pose is consistent with the PAL experiments showing the labeling of A329, a residue predicted to be part of the fatty acid tunnel. To refine the model of the ASCL4-**9** complex, molecular dynamics (MD) simulations were carried out during triplicated 100 computed nanoseconds (Figures 4 and S9). All criteria satisfied a convergence in terms of energy relaxation, stabilization of gyration radius of the ACSL4-ATP-**9** complex. During this 100 ns MD-based energy relaxation, compound **9** interacts by sustained hydrogen bonds with Q302 side chain and to a lesser extent with the backbone of G443. Other interatomic attractions are hydrophobic contacts with the lipophilic tunnel exhibiting residues L325, V324, A329, L440, V477 and L468 (Figures 4 and S9).

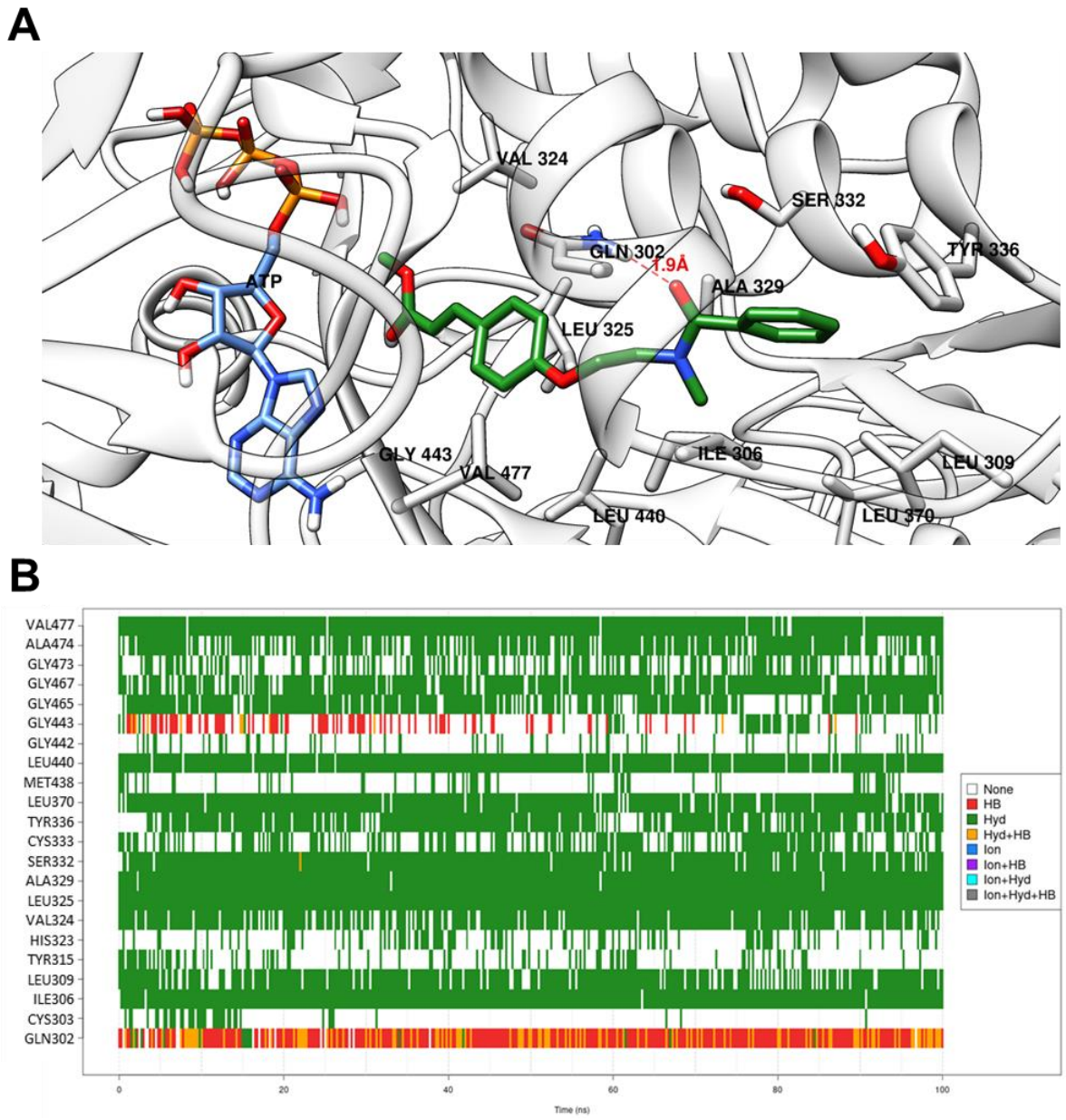

Figure 4. Putative binding mode of compound **9** on ACSL4. **A**) ASCL4-compound **9** complex after docking and an additional 100 ns MD simulation. **B**) Representative trace of the contacts that compound **9** forms with the ACSL4 model during the 100 ns MD simulation, showing that compound **9** primarily interacts through hydrophobic contacts and hydrogen bonds with Q302. Each vertical line correspond to an intermolecular contact and the color is associated to the interaction type (*e.g.* green corresponds to a hydrophobic contact and red to a hydrogen bond).

Interestingly, among ACSLs, only ACSL4 exhibits a glutamine at position 302 (Figure S4). In contrast, ACSL3, for which compound **9** does not display any inhibitory activity, displays a methionine at this position. Thus, to verify the significance of Q302 in the potency and affinity of compound **9** for ACSL4, ACSL4(Q302A) and ACSL4(Q302M) mutants were generated, and their enzymatic activities evaluated (Figure S10). Only

the ACSL4(Q302M) protein exhibited activity comparable to wild-type ACSL4, whereas ACSL4(Q302A) maintained about 80% of the enzymatic activity.

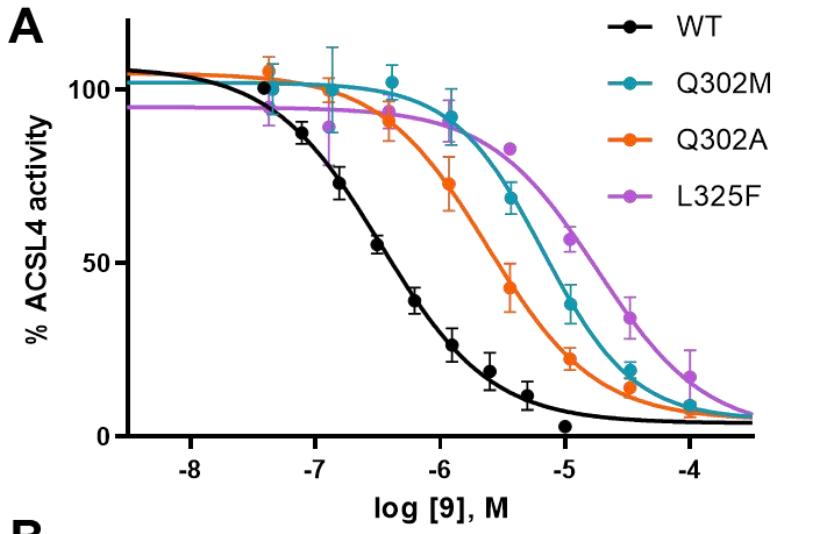

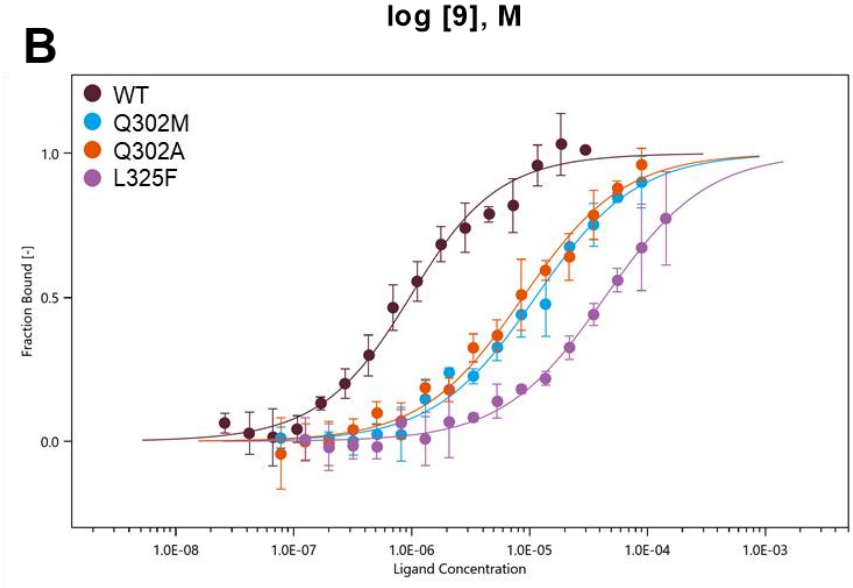

C

ACSL4	IC_{50} (µM)	K_D (µM)
WT	0.38 ± 0.03	0.72 ± 0.12
Q302M	7.1 ± 0.6	11.0 ± 1.6
Q302A	2.4 ± 0.4	8.6 ± 1.3
L325F	17.8 ± 3.8	43.5 ± 5.4

Figure 5. Impact of site-directed mutations on the inhibitory activity and affinity of compound **9** for ACSL4. **A**) Inhibition profiles of compound **9** against wild-type ACSL4 and selected mutants (Q302A in orange, Q302M in blue and L325F in purple) showing that the site-directed mutations affect inhibitory activity of **9**. **B**) Binding curves from MST experiments showing the impact of site-directed mutations (Q302A in orange, Q302M in blue and L325F in purple) on the affinity of compound **9** for ACSL4. **C**) Table summarizing IC_{50} and K_D values (± SEM) of compound **9** against wild-type ACSL4 and selected mutants.

To our satisfaction, introduction of the ACSL4(Q302M) mutation increased the IC_{50} value of **9** by 18-fold (IC_{50} ACSL4(Q302M) = 7.1 µM) and the K_D value by 15-fold, confirming the importance of Q302 in the binding of **9** (Figure 5). Similar trend was observed with ACSL4(Q302A). Additionally, we mutated L325 since this residue is predicted to be located in the middle of the FA tunnel. This residue is part of both identified peptides A and C and was shown to be important for the binding of **9** through hydrophobic interactions with the central phenyl ring. Interestingly, ACSL1, 5 and 6 display a phenylalanine residue at this position. Thus, we investigated ACSL4(L325F) mutant assuming that the bulky phenylalanine would sterically affect the binding of **9** into the FA tunnel. The ACSL4(L325F) mutant maintained about 60% activity (Figure S10) and introduction of this mutation led to around 50-fold increase of IC_{50} and K_D values for **9**. These results further corroborate the binding of **9** into the FA tunnel.

In summary, starting from the structure of ROSI, we designed novel sub-micromolar ACSL4 inhibitors that are selective against ACSL3 and devoid of PPARγ activity. We demonstrated that the binding of **9**, our best compound in this series, is dependent on the prior binding of ATP to ACSL4. HDx-MS experiments indicated that ATP binding induces a significant stabilization of the *C*-terminus domain. This effect was even more pronounced in the presence of **9** which further impacted the conformation of two other peptide sequences, one of which (peptide A) delineates the fatty acid gate-domain. PAL experiments based on diazirine-based probe **10** pinpointed residue A329, an amino acid predicted to be part of the fatty acid pocket. Complementary MD simulations pointed residue Q302 as a key amino acid for the binding of **9** through H-bonding. Site-directed mutagenesis supported this hypothesis, as mutation of Q302 induced a significant decrease in the potency and affinity of **9** to ACSL4. Compound **9** (**LIBX-A401**) therefore stands as a promising novel pharmacological tool to study the implication of ACSL4 in ferroptosis-related pathologies and cancer. Finally, the identification of the binding site of **9** (**LIBX-A401**) to ACSL4 paves the way to the rational design of ACSL4 inhibitors.

ACKNOWLEDGMENT

The authors thank Prof. Jean-François Goossens for providing access to the Varioskan Flash spectrophotometer. The 500 MHz and 300 MHz NMR facilities were funded by the Région Haut-de-France, the Fonds Européens de Développement

Régional (FEDER), the Ministère de l'Enseignement supérieur, de la Recherche et de l'Innovation (MESRI), and Université de Lille. The HDx-MS platform was supported by a grant from the Fondation Contre le Cancer (Ref: 3758) awarded to S.N.C. This work was supported by l'agence nationale de la recherche (ANR-23-CE18-0051) (EGID ANR-10-LABX-046), the French Community of Belgium (ARC 21/26-115), the Belgian Fonds National de la Recherche Scientifique (F.R.S.-FNRS; PDR grant 40003810), the Télévie (Grant 40007387). E.C. is a recipient of a Ph.D fellowship from the University of Lille and the Region Hauts-de-France. D.M.D. is a Télévie research fellow. N.P. received an Aspirant Ph.D Fellowship from FRS-FNRS (Belgium).

CONFLICT OF INTEREST

The authors declare no conflict of interest.

DATA AVAILABILITY STATEMENT

The data that support the findings of this study are available in the supplementary material of this article. This also includes further references.[21-26]

AUTHOR CONTRIBUTIONS

Darius Mazhari Dorooee: Conceptualization, Methodology, Formal analysis, Investigation, Data curation, Writing-original draft, Visualization.
Séverine Ravez: Conceptualization, Validation, Formal analysis, Investigation, Data curation, Writing-original draft, Writing – review & editing, Visualization, Supervision, Project administration, Funding acquisition.
Didier Vertommen: Methodology, Validation, Formal analysis, Investigation, Data curation, Supervision.
Nicolas Renault: Methodology, Validation, Formal analysis, Investigation, Data curation, Writing-original draft, Visualization.
Nicolas Papadopoulos: Methodology, Formal analysis, Investigation, Data curation.
Romain Marteau: Formal analysis, Investigation, Data curation.
Emeline Charnelle: Formal analysis, Investigation, Data curation.
Karine Porte: Formal analysis, Investigation, Data curation.
Alexandre Gobert: Formal analysis, Investigation, Data curation.

Nathalie Hennuyer: Formal analysis, Investigation, Data curation.

Gaetan Herinckx: Investigation, Data curation.

Bart Staels: Writing – review & editing, Funding acquisition.

Patricia Melnyk: Writing – review & editing, Funding acquisition.

Stefan N Constantinescu: Writing – review & editing, Funding acquisition.

Raphaël Frederick: Conceptualization, Validation, Writing – review & editing, Supervision, Project administration, Funding acquisition.

Jamal El Bakali: Conceptualization, Validation, Formal analysis, Investigation, Data curation, Writing-original draft, Writing – review & editing, Visualization, Supervision, Project administration, Funding acquisition.

REFERENCES

[1] T. J. Grevengoed, E. L. Klett, R.A Coleman, *Annu. Rev. Nutr.* **2014**, *34*, 1–30.

[2] a) P. A. Watkins, D. Maiguel, Z. Jia, J. Pevsner, *J. Lipid. Res.* **2007**, *48*, 2736-2750; b) E. Soupene, F. A. Kuypers, *Exp. Biol. Med. (Maywood)*. **2008**, *233*, 507–521; C) E. L. Klett, S. Chen, A. Yechoor, F. B. Lih, R. A. Coleman, *J. Lipid. Res.* **2017**, *58*, 884–894.

[3] a) J. Quan, A. M. Bode, X. Luo, *Eur. J. Pharmacol.* **2021**, *909*, 174397; b) Z. Wu, J. Sun, Z. Liao, J. Qiao, C. Chen, C. Ling, H. Wang, *Front. Neurosci.* **2022**, *16*, 1030512.

[4] J. Grube, M.M. Woitok, A. Mohs, S. Erschfeld, C. Lynen, C. Trautwein, T. Otto, *Cell Death Dis.* **2022**, *13*, 704.

[5] a) Y. Qiu, X. Wang, Y. Sun, T. Jin, R . Tang, X. Zhou, M. Xu, Y. Gan, R. Wang, H. Luo, M. Liu, X. Tang, *Cancer Res.* **2024**, *84*, 1856-1871; b) M. E. Monaco, *Oncotarget* **2023**, *14*, 563–575; c) J. Lin, P. Zhang, W. Liu, G Liu, J Zhang, M Yan, Y Duan, N.Yang, *Elife* **2023**, *12*, RP87510.

[6] a) Y. Ma, X. Zhang, O. A. Alsaidan, X. Yang, E. Sulejmani, J. Zha, Z. Beharry, H. Huang, M. Bartlett, Z. Lewis, H. Cai, *Mol. Cancer Res.* **2021**, *19*, 124–135. b) A. F. Castillo, U. D. Orlando, P. M. Maloberti, J. G. Prada, M. A. Dattilo, A. R. Solano, M. M. Bigi, M. A. Ríos Medrano, M. T. Torres, S. Indo, G. Caroca, H. R. Contreras, B. E. Marelli, F. J. Salinas, N. R. Salvetti, H. H. Ortega, P. Lorenzano Menna, S. Szajnman, D. E. Gomez, J. B. Rodríguez, E. J. Podesta, *Cell Mol. Life Sci.* **2021**, 78, 2893–2910. c) P. H. A. Cao, A. Dominic, F. E. Lujan, S. Senthilkumar, P. K. Bhattacharya, D. E. Frigo, E. Subramani, *Nat. Rev. Urol.* **2024**, doi: 10.1038/s41585-024-00869-9.

[7] a) S. J. Dixon, G. E. Winter, L. S. Musavi, E. D. Lee, B. Snijder, M. Rebsamen, G. Superti-Furga, B. R. Stockwell, *ACS Chem Biol.* **2015**, *10*, 1604–1609. b) H. Yuan, X. Li, X. Zhang, R. Kang, D.Tang *Biochem Biophys Res Commun.* **2016**, *478*, 1338–1343. c) S. Doll, B. Proneth, Y. Y. Tyurina, E. Panzilius, S. Kobayashi, I. Ingold, M. Irmler, J. Beckers, M. Aichler, A. Walch, H. Prokisch, D. Trümbach, G. Mao, F. Qu, H. Bayir, J. Füllekrug, C. H. Scheel, W. Wurst, J. A. Schick, V. E. Kagan, J. P. Angeli, Conrad M. *Nat. Chem. Biol.* **2017**, *13*, 91–98.

[8] a) S. J. Dixon, K. M. Lemberg, M. R. Lamprecht, R. Skouta, E. M. Zaitsev, C. E. Gleason, D. N. Patel, A. J. Bauer, A. M. Cantley, W. S. Yang, B. Morrison 3rd, B. R. Stockwell, *Cell* **2012**, *149*, 1060-1072. b) B. R. Stockwell, *Cell* **2022**, *185*, 2401–2421.

[9] V. E. Kagan, G. Mao, F. Qu, J. P. Angeli, S. Doll, C. S. Croix, H. H. Dar, B. Liu, V. A. Tyurin, V. B. Ritov, A. A. Kapralov, A. A. Amoscato, J. Jiang, T. Anthonymuthu, D. Mohammadyani, Q. Yang, B. Proneth, J. Klein-Seetharaman, S. Watkins, I. Bahar, J. Greenberger, R. K. Mallampalli, B. R. Stockwell, Y. Y.Tyurina, M. Conrad, H. Bayır, *Nat. Chem. Biol.* **2017**, *13*, 81–90.

[10] H. L. Zhang, B. X. Hu, Z. L. Li, T. Du, J. L. Shan, Z. P. Ye, X. D. Peng, X. Li, Y. Huang, X. Y. Zhu, Y. H. Chen, G. K. Feng, D. Yang, R. Deng, X. F. Zhu, *Nat. Cell. Biol.* **2022**, 24, 88–98.

[11] J. H. Kim, T. M. Lewin, R. A. Coleman, *J. Biol. Chem.* **2001**, *276*, 24667–24673.

[12] Y. Hisanaga, H. Ago, N. Nakagawa, K. Hamada, K. Ida, M. Yamamoto, T. Hori, Y. Arii, M. Sugahara, S. Kuramitsu, S. Yokoyama, M. Miyano, *J. Biol. Chem.* **2004**, *23*, 31717–31726.

[13] P. A. Watkins, D. Maiguel, Z. Jia, J. Pevsner, *J. Lipid. Res.* **2007**, *48*, 2736–2750.

[14] a) D. D. Weis, Hydrogen Exchange Mass Spectrometry of Proteins (John Wiley & Sons, 2016); b) L. Konermann, J. Pan, Y. H. Liu, *Chem. Soc. Rev.* **2011**, *40*, 1224–1234

[15] a) E. Smith, I. Collins, *Future Med. Chem.* **2015**, 159–183. b) O. Laselva, Z. Qureshi, Z. W. Zeng, E. V. Petrotchenko, M. Ramjeesingh, C. M. Hamilton, L. J. Huan, C. H. Borchers, R. Pomès, R. Young, C. E. Bear, *iScience* **2021**, *24*, 102542.

[16] R. Marteau, S. Ravez, D. Mazhari Dorooee, H. Bouchaoui, K. Porte, J. C. Devedjian, P. Melnyk, D. Devos, R. Frédérick, J. El Bakali, *Biochem. Pharmacol.* **2022**, *204*, 115239.

[17] K. Liu, R.M. Black, J. J. Acton 3rd, R. Mosley, S. Debenham, R. Abola, M. Yang, R. Tschirret-Guth, L. Colwell, C. Liu, M. Wu, C. F. Wang, K. L. MacNaul, M. E. McCann, D. E. Moller, J. P. Berger, P. T. Meinke, A. B. Jones, H. B. Wood, *Bioorg. Med. Chem. Lett.* **2005** , *15*, 2437–2440.

[18] G. R. Masson, J. E. Burke, N. G. Ahn, G. S. Anand, C. Borchers, S. Brier, G. M. Bou-Assaf, J. R. Engen, S. W. Englander, J. Faber, R. Garlish, P. R. Griffin, M. L. Gross, M. Guttman, Y. Hamuro, A. J. R. Heck, D. Houde, R. E. Iacob, T. J. D. Jørgensen, I. A. Kaltashov, J. P. Klinman, L. Konermann, P. Man, L. Mayne, B. D. Pascal, D. Reichmann, M. Skehel, J. Snijder, T. S. Strutzenberg, E. S. Underbakke, C. Wagner, T. E. Wales, B. T. Walters, D. D. Weis, D. J. Wilson, P. L. Wintrode, Z. Zhang, J. Zheng, D. C. Schriemer, K. D. Rand, *Nat. Methods* **2019**, *6*, 595–602.

[19] L. Stinnett, T. M Lewin, R. A.Coleman, *Biochim. Biophys. Acta* **2007**,*1771*, 119–125.

[20] J. Jumper, R. Evans, A. Pritzel, T. Green, M. Figurnov, O. Ronneberger, K. Tunyasuvunakool, R. Bates, A. Žídek, A. Potapenko, A. Bridgland, C. Meyer, S.A.A. Kohl, A.J. Ballard, A. Cowie, B. Romera-Paredes, S. Nikolov, R. Jain, J. Adler, T. Back, S. Petersen, D. Reiman, E. Clancy, M. Zielinski, M. Steinegger, M. Pacholska, T. Berghammer, S. Bodenstein, D. Silver, O. Vinyals, A.W. Senior, K. Kavukcuoglu, P. Kohli, D. Hassabis, *Nature* **2021**, *596*, 583–589.

[21] B. Staels, W. Koenig, A. Habib, R. Merval, M. Lebret, I. Pineda Torra, P. Delerive, A. Fadel, G. Chinetti, J.C. Fruchart, J. Najib, J. Maclouf, A. *Nature* **1998**, *393*, 790–793.

[22] C. V. Goemans, D. Vertommen, R. Agrebi, J.F. Collet, *Mol. Cell* **2018**, *70*, 614–627.

[23] A. T. McNutt, P. Francoeur, R. Aggarwal, T. Masuda, R. Meli, M. Ragoza, J. Sunseri, D.R.Koes, *J. Cheminform.* **2021**, *13*, 43.

[24] E. Krieger, G. Vriend, *Bioinformatics* **2014**, *30*, 2981–2982.

[25] S. L. Gaonkar, H. Shimizu, *Tetrahedron* **2010**, *66*, 3314–3317.

[26] R. G. Giles, N. J. Lewis, J. K. Quick, M. J. Sasse, M. W. J. Urquhart, L. Youssef, *Tetrahedron* **2000**, *56*, 4531–4537.